JCI The Journal of Clinical Investigation

Relieving Dyrk1a repression of MKL1 confers an adult-like phenotype to human infantile megakaryocytes

Kamaleldin E. Elagib, Ashton Brock, Cara M. Clementelli, Gohar Mosoyan, Lorrie L. Delehanty, Ranjit K. Sahu, Alexandra Pacheco-Benichou, Corinne Fruit, Thierry Besson, Stephan W. Morris, Koji Eto, Chintan Jobaliya, Deborah L. French, Paul Gadue, Sandeep Singh, Xinrui Shi, Fujun Qin, Robert Cornelison, Hui Li, Camelia Iancu-Rubin, Adam N. Goldfarb

J Clin Invest. 2022. https://doi.org/10.1172/JCI154839.

Research In-Press Preview **Development** **Hematology**

Graphical abstract

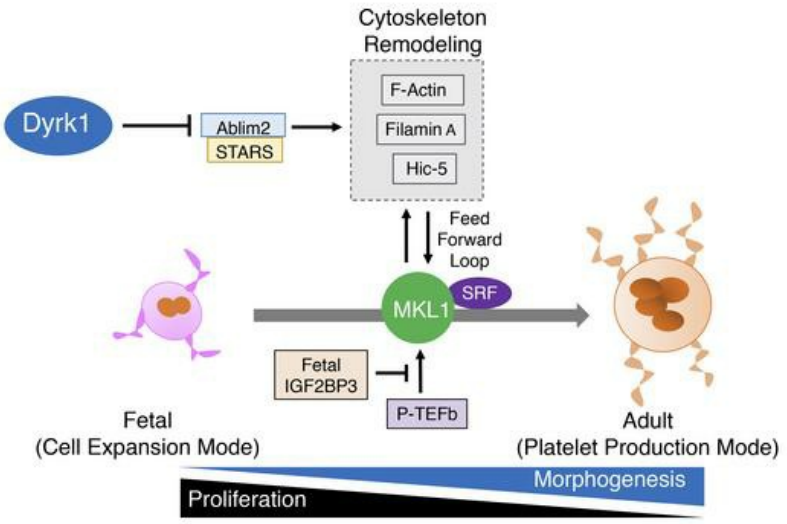

Title: Relieving Dyrk1a repression of MKL1 confers an adult-like phenotype to human infantile megakaryocytes

Authors: Kamaleldin E. Elagib[1], Ashton Brock[1], Cara Clementelli[2], Goar Mosoyan[2], Lorrie L. Delehanty[1], Ranjit K. Sahu[1], Alexandra Pacheco-Benichou[3], Corinne Fruit[3], Thierry Besson[3], Stephan W. Morris[4], Koji Eto[5], Chintan Jobaliya[6], Deborah L. French[6,7], Paul Gadue[6,7], Sandeep Singh[1], Xinrui Shi[1], Fujun Qin[1,8], Robert Cornelison[1], Hui Li[1], Camelia Iancu-Rubin[2,9], Adam N. Goldfarb[1]

Affiliations: [1]Department of Pathology, University of Virginia School of Medicine, Charlottesville, VA

[2]Tisch Cancer Institute, Department of Hematology and Medical Oncology, Icahn School of Medicine at Mount Sinai, New York, NY

[3]Normandie University, UNIROUEN, INSA Rouen, CNRS, COBRA UMR 6014, 76000, Rouen, France

[4]HealthChart LLC, Memphis, TN

[5]Center for iPS Cell Research and Application (CiRA), Kyoto University, Kyoto, Japan

[6]Center for Cellular and Molecular Therapeutics, The Children's Hospital of Philadelphia, Philadelphia, PA

[7]Department of Pathology and Laboratory Medicine, The Children's Hospital of Philadelphia, Philadelphia, PA

[8]Academy of Medical Sciences, School of Medicine, Zhengzhou University, Zhengzhou, Henan, China

[9] Department of Pathology, Molecular and Cell-Based Medicine, Icahn School of Medicine at Mount Sinai, New York, NY

Correspondence: Adam Goldfarb or Kamaleldin E. Elagib,

Department of Pathology, University of Virginia School of Medicine,

PO Box 800904, Charlottesville, Virginia 22908, USA.

Phone: 434.982.0593; E-mail: ang3x@virginia.edu (A. Goldfarb).

Phone: 434.982.0430; E-mail: ka8b@virginia.edu (K. Elagib)

Conflict of interest: The authors have declared that no conflict of interest exists.

Abstract

Infantile (fetal and neonatal) megakaryocytes have a distinct phenotype consisting of hyperproliferation, limited morphogenesis, and low platelet production capacity. These properties contribute to clinical problems that include thrombocytopenia in neonates, delayed platelet engraftment in recipients of cord blood stem cell transplants, and inefficient ex vivo platelet production from pluripotent stem cell-derived megakaryocytes. The infantile phenotype results from deficiency of the actin-regulated coactivator, MKL1, which programs cytoskeletal changes driving morphogenesis. As a strategy to complement this molecular defect, we screened pathways with potential to affect MKL1 function and found that Dyrk1a kinase inhibition dramatically enhanced megakaryocyte morphogenesis *in vitro* and *in vivo*. Dyrk1 inhibitors rescued enlargement, polyploidization, and thrombopoiesis in human neonatal megakaryocytes. Megakaryocytes derived from induced pluripotent stem cells responded in a similar manner. Progenitors undergoing Dyrk1 inhibition demonstrated filamentous actin assembly, MKL1 nuclear translocation, and modulation of MKL1 target genes. Loss of function studies confirmed MKL1 involvement in this morphogenetic pathway. Ablim2, a stabilizer of filamentous actin, increased with Dyrk1 inhibition, and Ablim2 knockdown abrogated the actin, MKL1, and morphogenetic responses to Dyrk1 inhibition. These results thus delineate a pharmacologically tractable morphogenetic pathway whose manipulation may alleviate clinical problems associated with the limited thrombopoietic capacity of infantile megakaryocytes.

Introduction

Human megakaryocytes undergo dramatic changes during ontogenic progression from fetal through adult stages. These changes include diminishing proliferation and a concomitant increase in adult-type morphogenesis (1-3). Adult-type morphogenesis comprises an orchestrated sequence of cellular transitions that enable efficient platelet production. This sequence of polyploidization, enlargement, and proplatelet formation stands apart from the core differentiation program of platelet protein and organelle induction, which is fully active throughout ontogeny (3, 4). The limited morphogenesis potential of infantile (fetal and neonatal) megakaryocytes has several clinical consequences, including the high incidence of thrombocytopenia in critically ill neonates and the delayed platelet engraftment in transplant patients receiving cord blood stem cells. Regarding neonatal thrombocytopenia, ~30% of newborns in Neonatal Intensive Care Units experience thrombocytopenia, the severity of which increases with prematurity; many receive platelet transfusions intended to diminish risk of intraventricular hemorrhage (1, 5). With allogeneic hematopoietic stem cell transplants, cord blood recipients experience a significant delay in platelet recovery as compared with adult progenitor recipients, leading to increased transfusions, as well as increased morbidity (1, 6, 7). Importantly, the cord blood recipients have similar numbers of marrow megakaryocytes as adult progenitor recipients, indicating a defect at the level of platelet production efficiency rather than megakaryocytic engraftment (8).

The limited capacity of infantile megakaryocytes for *ex vivo* platelet production also has clinical relevance. Global demographic trends predict worsening shortages of donor platelet units for transfusion, prompting a need for a donor-independent sources derived

from cultured megakaryocytes (9-12). Cord blood and pluripotent stem cell (PSC) megakaryocytes offer the only feasible sources for this application due to their capacity for large-scale expansion (10, 13, 14) and cryopreservation (15, 16). In addition, PSC-derived progenitors may undergo gene editing to produce HLA-null platelets (17), of particular importance due to the growing number of allo-sensitized patients requiring HLA-matched platelets (18). However, human PSC-derived megakaryocytes phenocopy those derived from fetal liver in their limited capacity for morphogenesis (19). Thus, a major obstacle to scaling up ex vivo platelet production for clinical usage consists of the low efficiency in thrombopoiesis. Development of specialized culture systems to replicate the mechanical and biophysical properties of the marrow milieu has improved platelet productivity (20-23). However, major limitations remain with scalability, cost effectiveness, limited platelet shelf life, and safety standards.

Within the process of morphogenesis, endomitosis leading to polyploidization plays a central role in determining platelet production capacity. Prior observations suggest that a single mature megakaryocyte after three rounds of endomitosis (16N) can yield ~125-fold more platelets than eight mature megakaryocytes produced by three standard mitoses (2N) (2). In adults, megakaryocytes can increase their polyploidization as part of the marrow response to increased platelet demand; the lack of such a capability in infants, on top of their lower basal ploidy, underlies their propensity to develop thrombocytopenia in response to a variety of stressors (1, 2). Hyperproliferation and impaired polyploidization also predispose infantile megakaryocytes to neoplastic transformation, explaining the occurrence of unique megakaryoblastic leukemias that appear only in early childhood (1, 24, 25).

Mechanisms governing ontogenic changes in megakaryocyte morphogenesis remain ill-defined. Their molecular definition, at a basic level, will illuminate cellular events guiding the process of polyploidization. At a translational level, these mechanisms will provide targets for treatment of thrombocytopenias associated with infantile megakaryocytes and approaches for scale-up of *ex vivo* platelet production. Along these lines, recent studies have implicated the onco-fetal RNA-binding protein IGF2BP3 as a driver of the infantile phenotype, acting to restrain morphogenesis through repression of MKL1 levels (26, 27). MKL1 (megakaryoblastic leukemia 1, also known as MRTFA) functions as a coactivator of the SRF (serum response factor) transcription factor in programming differentiation of multiple cell types including multiple muscle and hematopoietic lineages. It exerts these functions through control of genes involved in actin cytoskeleton remodeling and is in turn regulated by cytoskeletal status, with monomeric G-actin (globular) preventing its nuclear localization (28). MKL1 plays a critical role in driving adult megakaryocyte morphogenesis and undergoes upregulation and nuclear translocation in response to the megakaryopoietic cytokine thrombopoietin (28-30).

Experiments herein identify an approach to bypass the morphogenetic blockade imposed by IGF2BP3 in infantile megakaryocytes, applying a strategy of MKL1 potentiation. In screening of MKL1 regulatory pathways, we found that inhibition of Dyrk (dual-specificity tyrosine-regulated) kinase uniquely exerted a phenotypic and molecular rescue: 1) eliciting adult-type morphogenesis in neonatal and iPSC-derived (induced PSC) megakaryocyte progenitors, 2) enhancing neonatal platelet production both *in vitro* and *in vivo*, and 3) inducing via actin signaling the sustained nuclear translocation of

MKL1 associated with upregulation of MKL1/SRF target factors. Multiple approaches indicated specific involvement of the Dyrk1a isoform, which has previously been linked to megakaryocyte leukemogenesis in Down syndrome (31). A critical downstream effector in this pathway was identified as the F-actin (filamentous) stabilizer Ablim2 (actin-binding LIM protein 2), whose levels were controlled by Dyrk kinase activity and whose knockdown abrogated the response to Dyrk inhibition. These results thus identify molecular circuitry in megakaryocyte morphogenesis that participates in ontogenic programming and offers potential for therapeutic intervention.

Results

The morphogenesis blockade in infantile megakaryocytes is abrogated by Dyrk kinase inhibition. Deficient MKL1 expression contributes to the impaired morphogenesis of infantile megakaryocytes (26). To determine whether a strategy of functional enhancement could compensate for this deficiency, neonatal progenitors consisting of umbilical cord blood CD34+ cells underwent screening with inhibitors of kinases reported to restrain MKL1 activity (32-36). These experiments revealed that Dyrk kinase inhibition using harmine, a potent Dyrk inhibitor, uniquely and strongly enhanced morphogenesis, as reflected by induction of polyploidization (PI [propidium iodide]), enlargement (FSC [forward scatter]), cytoplasmic complexity (SSC [side scatter]), and morphologic features (Figure 1, A-D and Supplemental Figure 1, A-B). Treatment with this inhibitor had no effect on megakaryocytic commitment as reflected by percentage of CD41+ cells but did diminish overall number of cells by ~2-fold (Supplemental Figure 1C). Harmine also suppressed an infantile megakaryocyte feature, leaky expression of the erythroid marker GPA (glycophorin A) (26) (Supplemental Figure 1D). Analysis of a panel of compounds structurally related to harmine (37, 38) supported Dyrk1 kinases as the relevant target, rather than the non-kinase target monoamine oxidase (Supplemental Figure 2, A-B). A broad kinome screen has shown harmine to be highly restricted in its targets, with significant inhibitory activity at 10 μM toward only ~5 related kinases (Dyrk1a, Dyrk1b, Dyrk2, Clk1, and Clk2) (39). Nevertheless, to minimize potential for off-target effects, we also subjected neonatal progenitors to additional Dyrk1 inhibitors, EHT 1610 and FC 162, with structures and binding modes completely unrelated to harmine (40, 41). Notably, EHT 1610 demonstrates exquisite specificity for Dyrk1 with a 10-fold higher IC50 for

Dyrk2 (40). Accordingly, EHT 1610 and FC 162 enhanced morphogenesis in infantile megakaryocytes in a manner similar to harmine (Figure 1, E-H and Supplemental Figure 2, C-D), consistent with Dyrk1 as the likely target. As with the harmine treatment, EHT did not affect percentage of CD41+ cells but decreased overall number by ~2-fold (Supplemental Figure 2C).

The morphogenetic effects of Dyrk1 inhibition on primary neonatal progenitors raised the possibility of extending this approach to additional, clinically applicable systems for *ex vivo* megakaryopoiesis wherein morphogenesis is limited. Human pluripotent stem cell-derived megakaryocytes correspond in ontogenic stage to fetal liver progenitors and have minimal capacity for morphogenesis, even less than neonatal progenitors (19). The amenability to personalization and gene editing, however, has made induced pluripotent stem cells (iPSC) a particularly desirable source for developing donor-independent platelets (17, 42). We therefore tested the effects of Dyrk1 inhibition on iPSC-derived megakaryocytes, generated as previously described (16). In this system, both harmine and EHT 1610 markedly augmented several parameters of morphogenesis, attaining polyploidization levels typical of adult megakaryocytes (Figure 2, A-C and Supplemental Figure 3A). Recently, conditional immortalization of iPSC-derived megakaryocytic progenitors has facilitated their large-scale expansion while maintaining potential for inducible platelet production (22, 43). The prototypic cell line derived in this manner, imMKCL, showed limited morphogenesis upon induction of differentiation but potently responded to Dyrk1 inhibition with attainment of adult-type levels of polyploidization (Figure 2, D-F and Supplemental Figure 3B). Efficient *ex vivo* progenitor expansion has also been accomplished by treating neonatal CD34+ cells with the aryl hydrocarbon

antagonist SR1 (44, 45). As expected, SR1-treated cord blood progenitors underwent extensive self-renewal, with CD34 retained on 80% of cells at eight days of expansion culture. When transferred into megakaryocytic differentiation medium, these cells demonstrated a near-complete morphogenesis blockade. This blockade was effectively reversed by Dyrk1 inhibitors (Supplemental Figure 4, A-E), supporting applicability of this approach in several distinct scalable culture systems with potential for donor-independent platelet production.

Dyrk kinase inhibition enhances platelet production in infantile megakaryocytes. Efficiency of thrombopoiesis, i.e. platelet production, correlates directly with morphogenetic capacity (2, 46). To examine the effects of Dyrk1 inhibition on neonatal thrombopoiesis, we first conducted *in vitro* platelet release assays, as previously described (26). These assays demonstrated significant enhancement by both inhibitors of platelet release from cord blood-derived megakaryocytes (Figure 3, A-B; megakaryocyte numbers in Supplemental Figure 5, A-B), correlating with the effects seen on morphogenesis. The resulting platelets demonstrated appropriate ultrastructural characteristics and agonist responsiveness (Supplemental Figure 5, C-D). For assessment of in vivo thrombopoiesis, our recently developed xenotransplantation assay was employed (15). Megakaryocytes derived from neonatal progenitors cultured 11 days in megakaryocytic media -/+ 2.5 μM harmine were injected by tail vein at 4 x 10^6 cells/mouse. At the time of injection, the samples had similar levels of purity (81-84% $CD41^+$) and maturity (42-49% $CD42^+$ $CD41^+$). Quantitation of human platelets in the peripheral blood over 24 hours showed markedly enhanced *in vivo* platelet release by the harmine treated megakaryocytes at 1 hour and 4 hours (Figure 3C). Prior studies have

shown that intravenous injection of human megakaryocytes into immunodeficient mice leads to their retention in pulmonary capillaries, where platelet production then takes place (10). In the current experiments, flow cytometry on lung tissue for human megakaryocytes demonstrated uniformity of entrapment between the groups at 1 and 4 hours, supporting the action of harmine to be enhancement of release (Figure 3D). To address whether *in vivo* platelet lifespan was affected by the *ex vivo* culture conditions, platelets released in cultures of control versus harmine-treated megakaryocytes were infused into immunodeficient mice. Flow cytometric quantitation of human platelets showed no significant differences in rate of decline based on prior *ex vivo* treatment (Supplemental Figure 5E).

Implication of the Dyrk1a isoform in megakaryocyte morphogenesis. Among the 5 Dyrk kinase isoforms, Dyrk1a has previously been linked to megakaryopoiesis, its overexpression in Down syndrome contributing to the megakaryoblastic proliferations associated with trisomy 21 (31). To examine the influence of Dyrk1a on megakaryocyte morphogenesis *in vivo*, we generated mice with lineage-selective deficiency by crossing *Dyrk1a*-floxed (47) and *Pf4*-Cre strains (48). Generation of either haplo-insufficiency or homozygous deletion enhanced polyploidization, size, and cytoplasmic complexity in marrow megakaryocytes (Figure 4, A-C). Histologic evaluation confirmed these changes in the haplo-insufficient *Pf4*-Cre;*Dyrk1a*$^{f/wt}$ mice (Figure 4D, see red arrows). In the homozygous *Pf4*-Cre;*Dyrk1a*$^{f/f}$ mice, frequent pyknotic megakaryocytes also occurred (Figure 4D, blue arrows), consistent with Dyrk1a contribution to cell survival (37). Haplo-insufficiency did not alter platelet counts or mean platelet volume (MPV), possibly due to homeostatic compensations *in vivo*; homozygous deletion decreased platelets and

increased MPV, possibly reflecting toxic effects (Supplemental Figure 6, A-B). Neither manipulation affected marrow megakaryocyte frequency (Supplemental Figure 6C).

In primary human progenitors, neonatal megakaryocytes had significantly higher expression of Dyrk1a protein than in adult cells (Supplemental Figure 7A). Retroviral enforcement of Dyrk1a in the adult progenitors impaired morphogenesis (ploidy and size) as well as platelet release (Supplemental Figure 7, B-E). Loss of function studies could not employ shRNA-mediated knockdown due to early growth arrest associated with Dyrk1a repression, consistent anti-proliferative effects seen with pharmacologic inhibitors (Supplemental Figures 1C and 2C). However, the progenitors did tolerate a dominant-negative approach, with retroviral enforcement of the kinase dead mutant Dyrk1a K188R enhancing morphogenesis in adult and neonatal megakaryocytes (Supplemental Figure 7, B-D, F-G). Thus, several approaches support involvement of the Dyrk1a isoform in megakaryocyte morphogenesis.

MKL1 mediates Dyrk1 control of megakaryocyte morphogenesis. We initially addressed a potential role for MKL1 downstream of Dyrk1 by monitoring expression of two morphogenetic factors induced during adult but not fetal megakaryocytic development (26). Both factors, Filamin A and Hic-5, are encoded by MKL1 target genes (49-51). Immunoblotting showed significant enhancement of Filamin A and Hic-5 levels in neonatal megakaryocytes subjected to Dyrk inhibition (Figure 5, A-B), with similar responses observed in the iPSC-derived imMKCL line (Supplemental Figure 8A). These experiments demonstrated no effect of Dyrk inhibition on the upstream components of the ontogenic signaling pathway controlling MKL1 (26), P-TEFb and IGF2BP3 (Figure 5, A-B). P-TEFb activity in these experiments is reported by the levels of its target HEXIM1

(52-54), which increases in the physiologic fetal-adult megakaryocyte transition (26). To gain a broader picture of transcript alterations, purified early-stage megakaryocytes underwent RNA-seq analysis. Genes differentially expressed between adult and neonatal progenitors, i.e. ontogenic genes, were compared with genes affected by Dyrk inhibition, the latter defined as genes similarly regulated by harmine and EHT 1610 (Supplemental Figure 8B). Application of a hypergeometric distribution to quantitate enrichment confirmed significant overlap between ontogenic and Dyrk-related genes, both for upregulation and downregulation; in addition, genes upregulated by Dyrk inhibitors significantly overlapped with canonical MKL1 targets (55) (Figure 5C; see Supplemental Table 1 for gene lists with overlap in red). Gene set enrichment analysis by the Enrichr program (56) was also applied to the genes similarly influenced by ontogenic stage and Dyrk inhibitors. This approach identified actin-related features as the principal GO (gene ontology) categories enriched among the upregulated factors (Table 1). Of note, actin homeostasis has been designated as a conserved, core function of MKL1 (57). Among the commonly downregulated factors, early erythroid genes were identified as a leading category (Supplemental Table 2). Examining gene expression in more mature megakaryocytes (day 11), RNA-seq revealed *ACTB* (encoding β-actin) as a dominant factor upregulated by harmine (Supplemental Figure 8C), consistent with the notion of MKL1 and actin engaged in a feed-forward loop (28).

To determine the role of MKL1 in the morphogenetic effects of Dyrk inhibition, we cultured marrow progenitors from wild type and *Mkl1*-/- mice in megakaryocytic medium -/+ harmine. In these conditions, progenitors lacking MKL1 specifically lost the capacity for induction of polyploidization or enlargement, confirming its essential role in

responsiveness to Dyrk inhibition (Figure 5, D-F). Because Dyrk inhibitors did not affect overall levels of MKL1 (Figure 5, A-B), experiments addressed their effects on activity, which is controlled at the level of subcellular localization (58). Both Dyrk inhibitors induced a major redistribution of MKL1 on immunofluorescence from predominantly cytoplasmic to predominantly nuclear, observable in primary progenitors and in imMKCL cells (Figure 5, G-H and Supplemental Figure 8D). This effect was also discernable by biochemical fractionation (Supplemental Figure 8E). Note that in the primary progenitors, MKL1 localization (depicted in Figures 5G and 7D-E), as well as actin status (Figures 6A and 7G-H), were analyzed at 24 hours, prior to morphogenesis which was analyzed at 5 days. The rationale for this early analysis was to study early, upstream signaling events that could trigger morphogenesis, rather than later events that might occur secondary to morphogenesis.

Actin cytoskeletal remodeling is associated with Dyrk1 inhibition. MKL1 activity depends on the status of the actin cytoskeleton. Monomeric G-actin, through engagement of N-terminal RPEL motifs in MKL1, retains it in an inactive state in the cytoplasm; signaling via RhoA induces its nuclear translocation and activation by redistributing the actin into polymeric filaments (58). To monitor cytoskeletal changes, megakaryocyte progenitors subjected to Dyrk inhibition were assessed for filamentous actin (F-actin) content by staining with Phalloidin-594 and fluorescence microscopy. In primary human progenitors, as well as in the imMKCL line, both inhibitors strongly promoted actin incorporation into cortical filaments (Figure 6, A-B and Supplemental Figure 9A). A proteomic screen for Dyrk1a substrates previously implicated F-actin stabilizers in the Ablim family as potential downstream targets (33). Within this family,

Ablim2 demonstrated megakaryocyte-specific expression in human marrow samples and showed a cortical subcellular distribution pattern (ProteinAtlas database) (59). Treatment of neonatal progenitors with Dyrk1 inhibitors markedly augmented the levels of both Ablim2 and its cofactor STARS (striated muscle activator of Rho signaling) (60) (Figure 6, C-D and Supplemental Figure 9, B-C), with Ablim2 displaying a cortical distribution similar to that of F-actin (Supplemental Figure 9B). A connection between Dyrk1a and Ablim2 was further supported by retroviral transduction of adult progenitors in which enforcement of wild type Dyrk1a repressed Ablim2 levels while the dominant negative K188R enhanced its expression (Supplemental Figure 9D).

Ablim2 resides upstream of actin and MKL1 in morphogenesis signaling. Because of its role in F-actin stabilization and its control by Dyrk1 activity, Ablim2 was assessed for its participation in the morphogenetic effects of Dyrk inhibition. Neonatal CD34+ progenitors underwent lentiviral shRNA-mediated knockdowns (LV-shKD), using a standard approach in our lab (26). Two distinct hairpins each provided >80% knockdown (Supplemental Figure 10A), and both strongly suppressed polyploidization induced by Dyrk inhibitors (Figure 7, A-C). Ablim2 deficiency also blocked Filamin A induction as well as cytologic changes (Supplemental Figure 10, B-C). To determine the position of Ablim2 within the morphogenesis signaling pathway, we examined its influence on MKL1 and actin. Notably, knockdown of Ablim2 prevented both MKL1 nuclear translocation and F-actin formation in response to Dyrk inhibition (Figure 7, D-I), indicating its role as a critical upstream component in this pathway.

Discussion

The changes in megakaryocytes that occur with ontogenic development most likely serve stage-specific physiologic needs, such as rapid expandability in early embryogenesis, a capacity for vascular and immune modulation during later embryonic development, and prevention of a hypercoagulable state in the maturing fetus (1, 5). However, infantile megakaryocytes, including those in neonates, are poorly suited for adult needs due to their limited capacity for platelet production. Defining pathways that control ontogenic phenotype offers potential benefits in a variety of clinical scenarios, including thrombocytopenias in newborns and cord blood transplant recipients, as well as in optimizing systems to manufacture donor-independent platelets. In the last scenario, a capacity for rapid and efficient induction of adult-type morphogenesis in infantile megakaryocytes would eliminate a major bottle-neck in *ex vivo* production of clinical grade platelets, i.e. inefficiency of scale-up.

As a critical node in the natural transition from human fetal to adult megakaryopoiesis (26), the transcriptional coactivator MKL1 represents a rational target for ontogenic manipulation. Its signaling properties also make MKL1 a compelling target for morphogenesis enhancement. Firstly, its activation may be amplified through feed-forward loops associated with cytoskeletal reconfiguration. Its transcriptional partner SRF programs focal adhesion and F-actin assembly (61), which then further enhances its own nuclear translocation and co-activation function. Its direct targets Filamin A and Hic-5, which are deficient in fetal Mk (26) and induced by Dyrk inhibition (Figure 5A-B), both augment MKL1 activity. Filamin A directly binds MKL1 to potentiate its response to F-actin formation (62) and also contributes to Mk polyploidization (63). Hic-5 exerts feed-

forward activity by promoting F-actin stress fiber maturation (51). Secondly, MKL1-SRF signaling may participate in lineage consolidation by limiting the potential of progenitors to adopt alternative differentiation pathways (64), potentially acting to suppress the leaky erythroid gene expression characteristic of fetal Mk (26, 65) (see also Supplemental Figure 1D). Recent single cell RNA sequencing studies of human Mk from yolk sac, fetal liver, and adult marrow have highlighted heterogeneity at all stages, identifying subpopulations dedicated to either immune, hemostatic or niche functions (66, 67). A comparison of yolk sac Mk with the later-stage fetal liver Mk identifies emergence in the latter of an MK4 subset that bears signatures of cell-substrate adhesion, TGFβ signaling, and induction of cytoskeletal factors including actin, MYL9, and vimentin (66). All of these signatures are associated with MKL1 activity (28), suggesting emergence of an incipient morphogenesis program during the transition from yolk sac to fetal liver.

Endogenous stimuli known to control MKL1 activity include receptor-mediated signal transduction, the mechanical milieu, and nuclear lamina properties (28). Receptor engagement by the megakaryopoietic cytokine thrombopoietin induces rapid and transient MKL1 nuclear translocation in primary murine megakaryocytic progenitors in suspension culture (30). Environmental matrix stiffness provides a mechanical stimulus that promotes megakaryocyte morphogenesis via myosin heavy chain 9 signaling to MKL1 (21). Other mechanical stimuli that enhance megakaryocyte morphogenesis, such as shear stress and turbulence (20, 22), most likely also exert effects through MKL1 activation. Nuclear lamina components lamin A/C and emerin dictate nuclear compliance, which in turn affects actin network dynamics, MKL1 distribution (68), and megakaryocytic developmental potential (69). The clinical syndrome of Hutchinson-Gilford progeria,

caused by mutant lamin A and enhanced nuclear envelope stiffness, includes significantly elevated platelet counts (70). Transgenic mouse studies directly demonstrate aberrant MKL1 activation by the progerin mutant of lamin A (71). Thus, several factors have been found to enhance megakaryocyte morphogenesis via MKL1 activation, further validating its importance as a target. However, these pathways lack sufficient potency for efficient ontogenic reprogramming and are not easily amenable to therapeutic manipulation.

The pathway identified herein enables control of an ontogenic switch by applying a novel strategy that targets molecular defects underlying infantile megakaryocyte morphogenesis. We previously identified IGF2BP3 blockade of MKL1 induction as a key mechanism restraining morphogenesis (26). The current study establishes an approach by which to bypass this blockade through reinforcement of MKL1 at the functional level (Figure 7J). Prior studies have identified negative control of MKL1 exerted by multiple kinases. ERK-mediated phosphorylation of MKL1 on serine 454, located within a highly conserved central region, strongly enhances its interaction with G-actin and nuclear export (32). GSK3β-mediated phosphorylation on conserved serine 467 of the MKL1 paralog Myocardin, corresponding to serine 458 in MKL1, interferes with transcriptional activation function (34). Additional MKL1 phospho-sites have been mapped by Panayiotou, some with negative and others with positive effects (36). This group also identified an inhibitory effect of classical protein kinase C (cPKC) on F-actin formation, acting to block MKL1 nuclear translocation (36). Schneider et al. identified a similar inhibitory effect of Dyrk1a on F-actin and MKL1, exerted by phosphorylation of Ablim proteins (33). In the current work, our screen ruled out participation of ERK, GSK3b and cPKC in the restraint of MKL1 function in infantile megakaryocytes (Figure S1A-B). Our

studies rather identified Dyrk1a as the critical morphogenetic brake in megakaryopoiesis and showed that its activity can be manipulated to optimize platelet production. Availability of USFDA-approved (United States Food and Drug Administration) Dyrk1a inhibitors will enable clinical trials in the near future. Toxicities observed with shRNA knockdown and biallelic knockout do raise the possibility that *in vivo* treatment with such inhibitors may have a narrow therapeutic window. However, *ex vivo* treatment strategies will likely allow greater flexibility. From a broader perspective, our results show that defining basic mechanisms governing fetal to adult transitions can yield targeted approaches toward treatment of common clinical problems such as thrombocytopenia.

Methods

Cell culture. Cryopreserved neonatal cord blood (CB) and adult peripheral blood (PB) $CD34^+$ primary human progenitors were purchased, thawed, pre-stimulated, and subjected to unilineage megakaryocyte (Mk) culture as previously described (26). Specifically, undifferentiated cells were expanded for 72 hours in prestimulation medium containing Iscove modified Dulbecco medium with 20% BITS 9500 (StemCell Technologies), 2 mM l-glutamine, 100 ng/ml stem cell factor (SCF), 100 ng/ml FLT3-ligand (FLT3L), 100 ng/ml TPO, and 20 ng/ml IL-3. Unilineage Mk cultures contained the same basal medium, but with cytokines consisting of 40 ng/ml TPO, 25 ng/ml SCF, 100 ng/ml stromal-derived factor-α, and used fibronectin-coated wells. Cytokines were purchased from PeproTech. For prolonged expansion of undifferentiated human multipotent progenitors, CB $CD34^+$ cells underwent 8 days culture in pre-stimulation medium supplemented with 1 μM StemRegenin 1 (SR1, Selleckchem). Human induced pluripotent stem cell (iPSC) derived Mk progenitors, from the labs of co-authors Deborah French and Paul Gadue, were generated as described (16). The cryopreserved iPSC-derived Mk progenitors were thawed and grown in SDF (serum-free differentiation) medium medium consisting of 75% Iscove's Modified Dulbecco's Medium (IMDM) with 25% Ham's F12 medium, 0.5X N-2 supplement (Thermo Fisher Scientific), 1X B-27 supplement minus vitamin A (Thermo Fisher), 0.05% bovine serum albumin (Sigma-Aldrich), 50 μg/ml ascorbic acid (Sigma), 450 μM 1-thioglycerol (Sigma), 100 ng/ml human thrombopoietin (TPO, PeproTech), and 25 ng/ml human stem cell factor (SCF, PeproTech). The iPSC-derived Mk cell line imMKCL TkDN-SEV2 clone 7, from the lab of co-author Dr. Koji Eto, was derived, cryopreserved, thawed, and expanded in

suspension culture with doxycycline as published (43). For differentiation, cells underwent transfer to a recently optimized doxycycline-free induction medium, as described (22). Inhibitors of the MKL1-regulatory kinases cPKC (Go6983), MEK (U0126), and GSK3 (TDZD8) were purchased from Cayman Chemical, dissolved in DMSO (dimethyl sulfoxide) and then diluted in culture medium to final concentrations. The other commercially available inhibitors harmine (Dyrk family), INDY (Dyrk1a/b), harmane (MAO [monoamine oxidase]), and harmaline (MAO) were purchased from Sigma, and similarly dissolved in DMSO and diluted. The highly selective Dyrk1a inhibitors, EHT 1610 and FC 162, were synthesized as described (40, 41). These compounds were also dissolved in DMSO prior to use at the indicated concentrations. For *ex vivo* cultures of murine progenitors, marrows from mice treated with 5-fluorouracil (see "Mice" section below) underwent erythrocyte depletion with Gibco™ ACK lysing buffer (ThermoFisher) followed by washing with cold PBS. To expand progenitors, cells were cultured one day in RPMI-1640 with 10% FBS, supplemented with murine cytokines from Peprotech (50 ng/ml SCF, 50 ng/ml Interleukin-6, 20 ng/ml Interleukin-3), as well as 50 μM 2-mercaptoethanol, 100 U/ml penicillin, and 100 U/ml streptomycin. For Mk differentiation cytokine composition was changed to 40 ng/ml human TPO plus 25 ng/ml murine SCF, and cultures continued for an additional 3 days.

Cell transduction and transfection. Retroviral expression constructs for wild type and dominant negative Dyrk1a (MIGR1-WtDyrk1a and MIGR1-Dyrk1aK188R) were kindly provided by Dr. John D. Crispino (Northwestern University Feinberg School of Medicine) (31). Production of retroviral supernatants by transient transfection of these plasmids, and matched parent vector, into packaging lines, followed by progenitor

transduction using repeated spinoculation occurred as previously described (26, 72). For flow cytometric assessment of morphogenesis and for immunofluorescence, transduced cells were cultured an additional 5 days in megakaryocytic (Mk) medium. For platelet release assays, transduced cells were cultured 11 days in Mk medium. Lentiviral constructs for shRNA-mediated knockdowns of *ABLIM2* consist of the pLKO.1 vectors produced by The RNAi Consortium (TRC): clone IDs TRCN0000146452 (A8) and TRCN0000146821 (A9) (Horizon Discovery). Production of lentiviral supernatants by transient co-transfection of pLKO.1 vectors with packaging plasmids into 293T cells, purchased from the American Type Culture Collection, followed by spinoculation of pre-expanded progenitors took place as per descriptions (26, 29). Post spinoculation cells underwent selection in pre-stimulation medium with 1.2 μg/ml puromycin for 3 days followed by differentiation for 5 days in Mk medium with 0.5 μg/ml puromycin.

Mice. All experiments were approved by the University of Virginia and Icahn School of Medicine at Mount Sinai Institutional Animal Care & Use Committees (IACUC) and performed in accordance with the institutional animal care guidelines. *Mkl1*-/- mice generated in the lab of Dr. Stephan Morris as described (73) were backcrossed onto C57BL/6 and provided by Dr. Diane Krause (Yale School of Medicine). *Dyrk1a*-floxed mice on a C57BL/6 background (C57BL/6-*Dyrk1a*^{tm1Jdc}/J) were purchased from Jackson Labs. The megakaryocytic deleter strain *Pf4*-Cre on a C57BL/6 background (C57BL/6-Tg(Pf4-icre)Q3Rsko/J) was purchased from Jackson Labs. Immunodeficient xeno-transplant recipients consisted of NOD/SCID IL-2Rγ-null mice (NOD.Cg-*Prkdc*^{scid} *Il2rg*^{tm1Wjl}/SzJ, referred to as NSG), also purchased from Jackson Labs. PCR genotyping of genomic DNA is described in Supplement. Procedures included injection of a single

intraperitoneal (IP) dose of 5-fluorouracil (Teva Pharmaceutical) at 75 mg/kg 7 days prior to marrow harvest for ex vivo Mk cultures. Transplantation of human CB Mk into NSG mice followed our recently described approach (15), as did the quantitation of human circulating platelets and human megakaryocytes trapped in lung. For infusion of platelets, the mice each received 8.5 x 10^6 platelets from day 11 megakaryocytic cultures of cord blood CD34+ cells; as a positive control, a separate cohort of mice were infused with the same number of normal donor platelets.

Flow cytometry analysis. Human and murine progenitors cultured in Mk medium were washed, stained for surface markers -/+ DNA content, and analyzed as recently published (26). For analysis of primary bone marrow Mk, murine bone marrows were harvested, processed, and labelled as described (26). For all flow studies, assessments of ploidy, size (FSC), and granularity (SSC) were conducted on gated viable, singlet, $CD41^+$ Mk; in retroviral transduction experiments the gating additionally included GFP^+ cells, and BV421 rather than FITC was the fluorochrome for staining CD41. For studies prior to June 2017, analytical software consisted of FlowJo (TreeStar); later studies employed FCS Express 6 (De Novo). For the *in vitro* platelet release assay, culture-derived platelets underwent isolation and flow cytometric quantitation as described (15, 26). For platelet activation assays, culture-derived platelets were treated with 40 μM thrombin receptor activating peptide 6 (TRAP-6) (Thermo Fisher Scientific), plus 100 μM adenosine 50-diphosphate (ADP) (Sigma Aldrich). Samples were then stained with anti-human CD61 and CD62P or the corresponding isotype controls (Becton-Dickinson) and subjected to flow cytometry (15). Donor-derived platelets were stimulated and labeled identically and utilized as controls.

Microscopy. For cytology by light microscopy, cells underwent cytospin at a density of 2.5 x 10^4 per glass slide followed by Wright stain (Sigma-Aldrich). For light microscopic histology, formalin-fixed decalcified paraffin-embedded mouse femora were sectioned at 4 μm, deparaffinized with EZ Prep™ (Ventana), and subjected to hematoxylin/eosin staining. For immunofluorescence (IF), cells underwent cytospin at a density of 4 x 10^4 per glass slide followed by fixation 10 minutes in 4% paraformaldehyde/PBS at room temperature. Cells were then washed twice with PBS, and permeabilized/blocked for 1 hour in blocking buffer (PBS with 2% FBS, 2% BSA, and 0.1% Triton X-100). Primary antibodies consisted of rabbit polyclonal anti-MKL1 (Bethyl Laboratories, A302-201A) at 1/100 or rabbit polyclonal anti-Ablim2 (Sigma-Aldrich, HPA035808) at 1/100 in blocking buffer applied overnight at 4° C. After 4 washes with blocking buffer, the secondary incubation consisted of blocking buffer with goat anti-rabbit Alexa-Fluor 488™ (ThermoFisher) at 1/300, DAPI, and (where indicated) Alexa Fluor-594-Phalloidin (Invitrogen) at 1/20 for 60 minutes at room temperature. Slides washed 4 times with blocking buffer and once with PBS underwent coverslip mounting with Vectashield medium (Vector Laboratories H-1000). Cytologic imaging by light microscopy employed an Olympus BX51 microscope equipped with an Olympus DP70 digital camera. Objective lenses consisted of Uplan Fl 20×/0.50 NA and Uplan Fl 40×/0.75 NA. Image acquisition and processing used Photoshop CS2/9.0 and CS3/10.0 (Adobe Systems, San Jose, CA) and Fiji (ImageJ V1, NIH). Histologic imaging by light microscopy employed a Hamamatsu NanoZoomer S360 scanner followed by processing with Fiji. For IF, single-plane mid-nucleus images were captured with a Zeiss LSM 700 confocal microscope using the 63X objective. Images were processed using Fiji. MKL1

nuclear signal was quantitated from the green signal that overlapped with DAPI. Cytoplasmic MKL1 was derived by subtracting green nuclear signal from pan-cellular green signal. To quantitate F-actin, signals from staining with phalloidin-Alexa-594 were divided by number of cells/field to yield cellular mean fluorescence intensity (MFI) using Fiji. For all IF experiments, $\geq$ 50 cells per experiment were used for quantitation. Transmission electron microscopy of culture-derived and normal donor platelets was conducted with a HitachiH-7650 transmission electron microscope (Hitachi High-Technologies Instrumentation, Tokyo, Japan) linked to a SIA (Scientific Instruments and Applications, Duluth, GA) digital camera (15).

Cell extraction, fractionation and immunoblot. Cultured imMKCL cells underwent washing with PBS, re-suspension in ice-cold Buffer A (10 mM HEPES-KOH pH 7.9, 1.5 mM $MgCl_2$, 10 mM KCl, 0.5 mM DTT, 0.2 mM PMSF, 1x cOmplete^{TM} EDTA-free protease inhibitor cocktail [Roche], 40 μM calpeptin [Sigma-Aldrich]), incubation for 10 minutes followed by vortexing for 10 seconds and pelleting with a 10 second microfuge pulse. The cell pellets were re-suspended in ice-cold Buffer B (10 mM HEPES-KOH pH 7.5, 10 mM $MgCl_2$, 10 mM KCl, 1 mM DTT, 1 mM EDTA, 1x protease inhibitor cocktail, 40 μM calpeptin and 0.2% NP-40), incubated for 10 minutes, and microfuged 5 minutes at 5000 rpm, with supernatants collected as “Cytoplasmic Fractions.” Pellets underwent washing with Buffer B and then re-suspension in ice cold Buffer C (20 mM HEPES-KOH pH 7.5, 1.5 mM $MgCl_2$, 450 mM NaCl, 1 mM DTT, 0.5 mM EDTA, 1x protease inhibitor cocktail, 40 μM calpeptin, and 0.5% NP-40), incubation 10 minutes, microfuge 5 minutes at 10,000 rpm, and collection of supernatants designated “Nuclear Fractions.” For immunoblotting, subcellular fractions were mixed with equal volumes of 2X Laemmli sample buffer (60 mM

Tris-HCl, pH 6.8, 2% SDS, 100 μM dithiothreitol, 10% glycerol, and 0.01% bromophenol blue). For direct analysis of whole cell lysates, intact cell pellets underwent lysis in an equal volume of 2X Laemmli supplemented with protease and phosphatase inhibitors (cOmplete and PhosSTOP, Roche) followed by shearing of DNA. All samples were boiled 5 minutes, followed by SDS-PAGE and immunoblot as described (74). Primary antibodies and incubation conditions are provided in Supplemental Table 3. Densitometry data were acquired on a GS800 calibrated densitometer (Bio-Rad) and analyzed with Quantity One software (Bio-Rad).

RNA sequencing. Adult and neonatal $CD34^+$ cells cultured in megakaryocytic medium 4 days with DMSO or Dyrk inhibitors underwent removal of dead cells by Ficoll gradient centrifugation (GE Healthcare Bio-Sciences AB, Uppsala, Sweden). Megakaryocytes were then purified using anti-CD61 microbeads (Miltenyi Biotec, Auburn, CA) combined with magnetic sorting on an autoMACS Pro Separator (Miltenyi). RNA isolation employed the RNeasy Plus Mini Kit (Qiagen, Hilden, Germany), followed by quality control using an Agilent 2100 (Agilent, Santa Clara, CA). The cDNA library was constructed using an NEBNext Ultra II RNA Library Prep Kit for Illumina (New England BioLabs, Ipswich, MA), and sequencing was conducted on an NovaSeq 6000 Sequencing System (Illumina, San Diego, CA). The raw sequencing data underwent quality control analysis and filtering using the NG SQC Tool Kit version 2.3.3, followed by alignment of high-quality reads to the hg38 genome using HISAT version 2.1.0, read count determination with StringTie version 1.3.3b, and differential expression analysis with Ballgown version 2.6.0 (75). Gene set enrichment analysis was conducted using Enrichr (56). Sequence files have been deposited in GEO (GSE195671).

Statistics. Individual results shown are representative of at least three independent experiments. Graphs were generated using GraphPad Prism version 9.1.2 and depict mean values from $\geq$ 3 independently conducted experiments ± standard error of the mean. Single, pairwise comparisons employed Student's *t* test, 1-tailed; multiple comparisons employed one way ANOVA with Tukey *post hoc* test using SPSS Statistics V26 (IBM). Gene set overlaps were analyzed using the Stat Trek Hypergeometric Calculator (https://stattrek.com/online-calculator/hypergeometric.aspx). A *P* value less than 0.05 was considered significant.

Study approval. $CD34^+$ cells purchased from the Fred Hutchinson Cancer Research Center, AllCells and StemCell Technologies were originally obtained from donors with informed consent and IRB approval at institutions of origin. Animal studies were approved and performed in compliance with the University of Virginia and Icahn School of Medicine/Mount Sinai IACUC committees and guidelines.

Author Contributions

K.E.E. performed experiments, conceptualized and interpreted data, and wrote the manuscript. A.B. performed cell culture experiments and assisted with mouse studies. G.M. and C.C. conducted NSG xenotransplantation and in vitro platelet release assays. L.L.D. assisted with mouse breeding and analysis. R.K.S. assisted with flow cytometry studies. A.P-B., C.F., and T.B. synthesized selective Dyrk1 inhibitors. S.W.M. generated the *Mkl1*-/- murine strain. K.E. developed the iPSC-derived imMKCL line. C.J., D.L.F., and P.G. developed the iPSC-derived megakaryocytes. C.I-R. supervised NSG

xenotransplantation and in vitro platelet release experiments and interpreted data. S.S., X.S., F.Q., and R.C. processed and analyzed RNA-seq data under the supervision of H.L. A.N.G. conceived and supervised the project, interpreted the data, and wrote the manuscript.

Acknowledgments

All of the authors thank John Crispino for providing plasmids; Joanne Lannigan and the UVA Flow Cytometry Core Facility for assistance with flow cytometry; Stacey Criswell and the UVA Advanced Microscopy Facility for assistance with confocal imaging; Nicole Brimer for guidance with quantitative image analysis; Pat Pramoonjago and Ashley Volaric for expert assistance with immunohistochemical analysis; John Luckey for helpful suggestions; Zollie White for reviewing the manuscript. A.P-B., C.F., and T.B. acknowledge the support of the University of Rouen Normandy, INSA Rouen, the Centre National de la Recherche Scientifique (CNRS), European Regional Development Fund (ERDF), Labex SynOrg (ANR-11-LABX-0029), Carnot Institute I2C, the graduate school for research XL-Chem (ANR-18-EURE-0020 XL CHEM), and Région Normandie. This work was supported by grants from the National Institutes of Health (R01 HL130550, R01 HL149667).

References

1. Davenport P, et al. Changes in megakaryopoiesis over ontogeny and their implications in health and disease. *Platelets.* 2020;31(6):692–9.
2. Mazzi S, et al. Megakaryocyte and polyploidization. *Exp Hematol.* 2018;57:1–13.
3. Davenport P, et al. Fetal vs adult megakaryopoiesis. *Blood.* 2022;139(22):3233–44.
4. Liu Z–J, et al. Developmental differences in megakaryocytopoiesis are associated with up–regulated TPO signaling through mTOR and elevated GATA–1 levels in neonatal megakaryocytes. *Blood.* 2011;117(15):4106–17.
5. Davenport P, and Sola–Visner M. Hemostatic challenges in neonates. *Front Pediatr.* 2021;9:627715 (1–14).
6. Tang B, et al. Recombinant human thrombopoietin promotes platelet engraftment after umbilical cord blood transplantation. *Blood Adv.* 2020;4(16):3829–39.
7. Solh M, et al. Platelet and red blood cell utilization and transfusion independence in umbilical cord blood and allogeneic peripheral blood hematopoietic cell transplants. *Biol Blood Marrow Transplant.* 2011;17(5):710–6.
8. Ignatz M, et al. Umbilical cord blood produces small megakaryocytes after transplantation. *Biol Blood Marrow Transplant.* 2007;13:145–50.
9. Cobain TJ, et al. A survey of the demographics of blood use. *Transfus Med.* 2007;17(1):1–15.
10. Gollomp K, et al. Current status of blood pharming: megakaryocyte transfusions as a source of platelets. *Curr Opin Hematol.* 2017;24:565–71.
11. Lambert MP, et al. Challenges and promises for the development of donor–independent platelet transfusions. *Blood.* 2013;121(17):3319–24.
12. Estcourt LJ. Why has demand for platelet components increased? A review. *Transfus Med.* 2014;24:260–8.
13. Tao H, et al. Cord blood is better than bone marrow for generating megakaryocytic progenitor cells. *Exp Hematol.* 1999;27:293–301.
14. Avanzi MP, et al. A novel bioreactor and culture method drives high yields of platelets from stem cells. *Transfusion.* 2016;56:170–8.
15. Patel A, et al. Pre–clinical development of a cryopreservable megakaryocytic cell product capable of sustained platelet production in mice. *Transfusion.* 2019;59:3698–713.
16. Sim X, et al. Identifying and enriching platelet–producing human stem cell–derived megakaryocytes using factor V uptake. *Blood.* 2017;130(2):192–204.

17. Suzuki D, et al. iPSC–derived platelets depleted of HLA class I are inert to anti–HLA class I and natural killer cell immunity. *Stem Cell Reports.* 2020;14:49–59.
18. Juskewitch JE, et al. How do I … manage the platelet transfusion–refractory patient? *Transfusion.* 2017;57:2828–35.
19. Bluteau O, et al. Developmental changes in human megakaryopoiesis. *J Thromb Haemost.* 2013;11:1730–41.
20. Thon JN, et al. Platelet Bioreactor–on–a–chip. *Blood.* 2014;124(12):1857–67.
21. Aguilar A, et al. Importance of environmental stiffness for megakaryocyte differentiation and proplatelet formation. *Blood.* 2016;128(16):2022–32.
22. Ito Y, et al. Turbulence activates platelet biogenesis to enable clinical scale *ex vivo* production. *Cell.* 2018;174:636–48.
23. Di Buduo CA, et al. Programmable 3D silk bone marrow niche for platelet generation ex vivo and modeling of megakaryopoiesis pathologies. *Blood.* 2015;125(14):2254–64.
24. de Rooij JDE, et al. Pediatric non–Down syndrome acute megakaryoblastic leukemia is characterized by distinct genomic subsets with varying outcomes. *Nature Gen.* 2017;49(3):451–6.
25. Gruber TA, and Downing JR. The biology of pediatric acute megakaryoblastic leukemia. *Blood.* 2015;126(8):943–9.
26. Elagib KE, et al. Neonatal expression of RNA–binding protein IGF2BP3 regulates the human fetal–adult megakaryocyte transition. *J Clin Invest.* 2017;127(6):2365–77.
27. Elagib KE, et al. Megakaryocyte ontogeny: Clinical and molecular significance. *Exp Hematol.* 2018;61:1–9.
28. Reed F, et al. MRTFA: A critical protein in normal and malignant hematopoiesis and beyond. *J Biol Chem.* 2021;296:100543 (2–37).
29. Elagib KE, et al. Calpain 2 activation of P–TEFb drives megakaryocyte morphogenesis and is disrupted by leukemogenic GATA1 mutation. *Dev Cell.* 2013;27:607–20.
30. Smith EC, et al. Induction of megakaryocyte differentiation drives nuclear accumulation and transcriptional function of MKL1 via actin polymerization and RhoA activation. *Blood.* 2013;121(7):1094–101.
31. Malinge S, et al. Increased dosage of the chromosome 21 ortholog *Dyrk1a* promotes megakaryoblastic leukemia in a murine model of Down syndrome. *J Clin Invest.* 2012;122(3):948–62.

32. Muehlich S, et al. Serum–induced phosphorylation of the serum response factor coactivator MKL1 by the extracellular signal–regulated kinase 1/2 pathway inhibits its nuclear localization. *Mol Cell Biol.* 2008;28(20):6302–13.
33. Schneider P, et al. Identification of a novel actin–dependent signal transducing module allows for the targeted degradation of GLI1. *Nat Commun.* 2015;6:8023 (1–15).
34. Badorff C, et al. Glycogen synthase kinase 3beta inhibits Myocardin–dependent transcription and hypertrophy induction through site–specific phosphorylation. *Circ Res.* 2005;97:645–54.
35. Charbonney E, et al. beta–Catenin and Smad3 regulate the activity and stability of myocardin–related transcription factor during epithelial–myofibroblast transition. *Mol Biol Cell.* 2011;22:4472–85.
36. Panayiotou R, et al. Phosphorylation acts positively and negatively to regulate MRTF–A subcellular localisation and activity. *eLife.* 2016;5:e15460.
37. Fernandez–Martinez P, et al. DYRK1A: the double–edged kinase as a protagonist in cell growth and tumorigenesis. *Mol Cell Onc.* 2015;2(1):e970048.
38. Waki H, et al. The small molecule harmine is an antidiabetic cell–type–specific regulator of PPARgamma expression. *Cell Metabol.* 2007;5:357–70.
39. Ackeifi C, et al. Pharmacologic and genetic approaches define human pancreatic beta cell mitogenic targets of DYRK1A inhibitors. *JCI Insight.* 2020;5(1):e132594.
40. Chaikuad A, et al. An unusual binding model of the methyl 9-anilinothiazolo[5,4-f] quinazoline–2–carbimidates (EHT 1610 and EHT 5372) confers high selectivity for dual–specificity tyrosine phosphorylation–regulated kinases. *J Med Chem.* 2016;59:10315–21.
41. Fruit C, et al. Biological characterization of 8–cyclopropyl–2–(pyridin–3–yl)thiazolo[5,4–f]quinazolin–9(8H)–one, a promising inhibitor of DYRK1A. *Pharmaceuticals.* 2019;12(4):E185.
42. Lyde RB, et al. Infused factor VIII–expressing platelets or megakaryocytes as a novel therapeutic strategy for hemophilia A. *Blood Adv.* 2019;3(9):1368–78.
43. Nakamura S, et al. Expandable megakaryocyte cell lines enable clinically applicable generaton of platelets from human induced pluripotent stem cells. *Cell Stem Cell.* 2014;14:535–48.
44. Boitano AE, et al. Aryl hydrocarbon receptor antagonists promote the expansion of human hematopoietic stem cells. *Science.* 2010;329:1345–8.

45. Wagner JE, et al. Phase I/II trial of StemRegenin-1 expanded umbilical cord blood hematopoietic stem cells supports testing as a stand-alone graft. *Cell Stem Cell.* 2016;18:144-55.
46. Mattia G, et al. Different ploidy levels of megakaryocytes generated from peripheral or cord blood CD34+ cells are correlated with different levels of platelet release. *Blood.* 2002;99(3):888-97.
47. Thompson BJ, et al. DYRK1A controls the transition from proliferation to quiescence during lymphoid development by destabilizing Cyclin D3. *J Exp Med.* 2015;212(6):723-40.
48. Tiedt R, et al. *Pf4-Cre* transgenic mice allow the generation of lineage-restricted gene knockouts for studying megakaryocyte and platelet function in vivo. *Blood.* 2007;109(4):1503-6.
49. Smith EC, et al. MKL1 and MKL2 play redundant and crucial roles in megakaryocyte maturation and platelet formation. *Blood.* 2012;120(11):2317-29.
50. Rahman N-T, et al. MRTFA augments megakaryocyte maturation by enhancing the SRF regulatory axis. *Blood Adv.* 2018;2(20):2691-703.
51. Varney SD, et al. Hic-5 is required for myofibroblast differentiation by regulating mechanically dependent MRTF-A nuclear accumulation. *J Cell Sci.* 2016;129:774-87.
52. He N, et al. Modulation of a P-TEFb functional equilibrium for the global control of cell growth and differentiation. *Mol Cell Biol.* 2006;26(19):7068-76.
53. Garriga J, et al. Selective control of gene expression by CDK9 in human cells. *J Cell Physiol.* 2010;222:200-8.
54. Bartholomeeusen K, et al. BET bromodomain inhibition activates transcription via a transient release of P-TEFb from 7SK snRNP. *J Biol Chem.* 2012;287(43):36609-16.
55. Esnault C, et al. Rho-actin signaling to the MRTF coactivators dominates the immediate transcriptional response to serum in fibroblasts. *Genes Dev.* 2014;28(9):943-58.
56. Xie Z, et al. Gene set knowledge discovery with Enrichr. *Curr Prot.* 2021;1:e90(1-51).
57. Salvany L, et al. The core and conserved role of MAL is homeostatic regulation of actin levels. *Genes Dev.* 2014;28:1048-53.
58. Posern G, and Treisman R. Actin'together: serum response factor, its cofactors and the link to signal transduction. *Trends Cell Biol.* 2006;16(11):588-96.
59. Uhlen M, et al. Tissue-based map of the human proteome. *Science.* 2015;347(6220):1260419-1-9.

60. Barrientos T, et al. Two novel members of the ABLIM protein family, ABLIM-2 and -3, associate with STARS and directly bind F-actin. *J Biol Chem.* 2007;282(11):8393-403.
61. Schratt G, et al. Serum response factor is crucial for actin cytoskeletal organization and focal adhesion assembly in embryonic stem cells. *J Cell Biol.* 2002;156(4):737-50.
62. Kircher P, et al. Filamin A interacts with the coactivator MKL1 to promote the activity of the transcription factor SRF and cell migration. *Sci Signal.* 2015;8(402):ra112.
63. Begonja AJ, et al. FlnA-null megakaryocytes prematurely release large and fragile platelets that circulate poorly. *Blood.* 2011;118(8):2285-95.
64. Ikeda T, et al. Srf destabilizes cellular identity by suppressing cell-type-specific gene expression programs. *Nat Commun.* 2018;9:1387 (1-15).
65. Woo AJ, et al. Developmental differences in IFN signaling affect GATA1s-induced megakaryocyte hyperproliferation. *J Clin Invest.* 2013;123(8):3292-304.
66. Wang H, et al. Decoding human megakaryocyte development. *Cell Stem Cell.* 2021;28:535-49.
67. Liu C, et al. Characterization of cellular heterogeneity and an immune subpopulation of human megakaryocytes. *Adv Sci.* 2021;8:2100921 (1-14).
68. Ho CY, et al. Lamin A/C and emerin regulate MKL1-SRF activity by modulating actin dynamics. *Nature.* 2013;497:507-11.
69. Shin J-W, et al. Lamins regulate cell trafficking and lineage maturation of adult human hematopoietic cells. *Proc Natl Acad Sci USA.* 2013;110(47):18892-7.
70. Merideth MA, et al. Phenotype and course of Hutchinson-Gilford progeria syndrome. *N Engl J Med.* 2008;358(6):592-604.
71. Osmanagic-Myers S, et al. Endothelial progerin causes cardiovascular pathology through an impaired mechanoresponse. *J Clin Invest.* 2019;129(2):531-45.
72. Elagib KE, et al. Jun blockade of erythropoiesis: role for repression of GATA-1 by HERP2. *Mol Cell Biol.* 2004;24(17):7779-94.
73. Sun Y, et al. Acute myeloid leukemia-associated *Mkl1 (Mrtf-a)* is a key regulator of mammary gland function. *Mol Cell Biol.* 2006;26(15):5809-26.
74. Elagib KE, et al. Cross-talk of GATA-1 and P-TEFb in megakaryocyte differentiation. *Blood.* 2008;112(13):4884-94.
75. Pertea M, et al. Transcript-level expression analysis of RNA-seq experiments with HISAT, StringTie and Ballgown. *Nat Protocols.* 2016;11(9):1650-67.

Figure 1

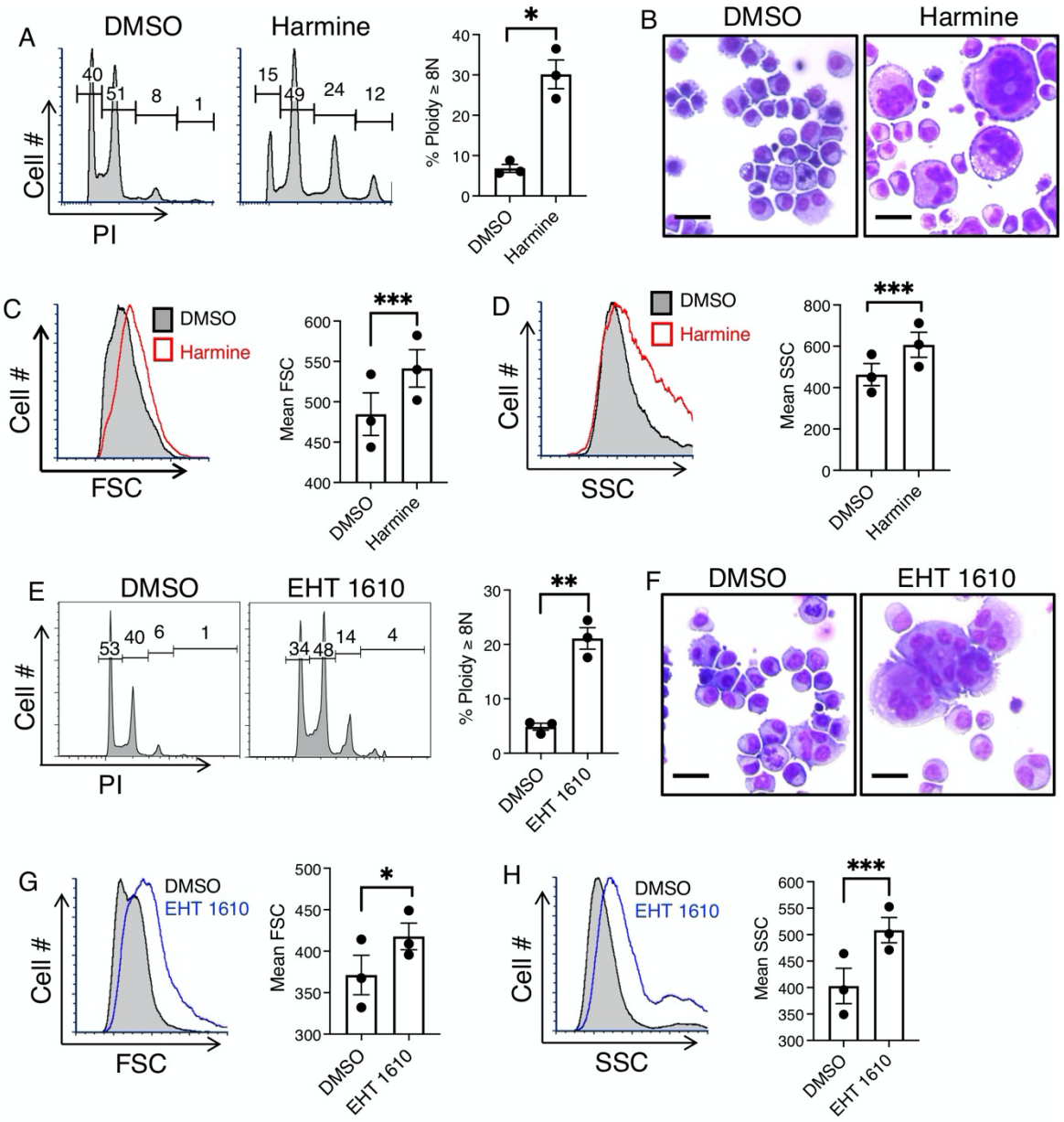

Figure 1. **Induction of adult-type morphogenesis in neonatal megakaryocytes (Mk) treated with Dyrk kinase inhibitors**. (**A-D**) Umbilical cord blood CD34$^+$ cells were cultured in Mk medium ± 5 µM Dyrk inhibitor harmine for 6 days. Cells were analyzed either by flow cytometry after costaining with FITC-anti-CD41 and propidium iodide (PI), or by microscopy of cytospins. (**A**) Mk polyploidization (PI). (**B**) Morphology of cytospins subjected to Wright stain and light microscopy (Olympus BX51 microscope, original magnification x 200, scale bar 20 µm). (**C**) Mk size (FSC). (**D**) Mk complexity/granulation (SSC). Graphs for **A-D**: mean ± SEM for 3 independent experiments. *P < 0.05; ***P < 0.005, Student's t test. (**E-H**) Cells cultured and analyzed as in (**A**) but ± 5 µM selective Dyrk1a inhibitor EHT 1610. (**E**) Mk polyploidization (PI). (**F**) Morphology in cytospins as in (**B**). (**G**) Mk size (FSC). (**H**) Mk complexity/granulation (SSC). Graphs for **E-H**: mean ± SEM for 3 independent experiments. *P < 0.05; **P < 0.01; ***P < 0.005, Student's t test.

Figure 2

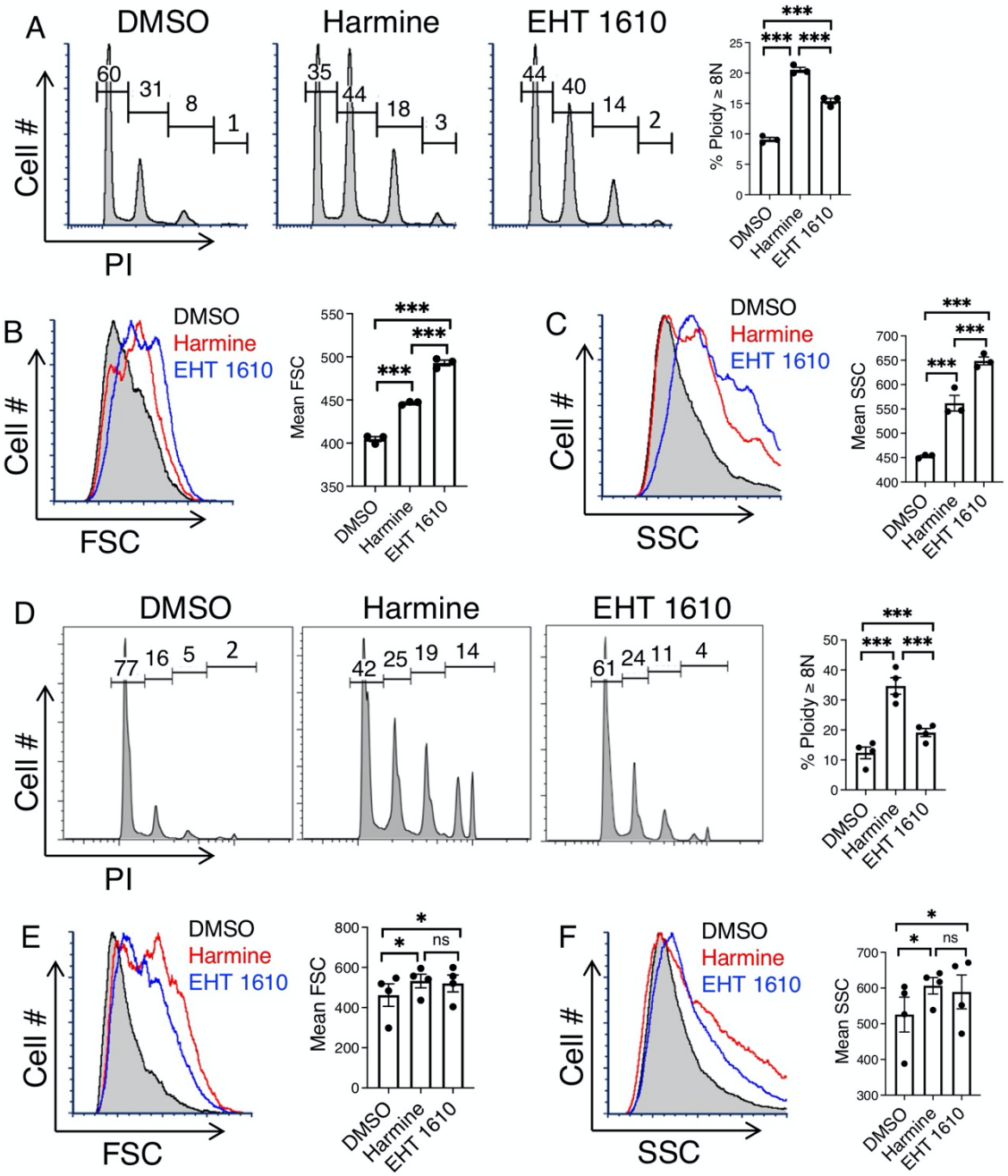

Figure 2. Dyrk1 inhibitors elicit adult-type morphogenesis in iPSC-derived megakaryocytes (Mk). (**A-C**) Human iPSC-derived Mk progenitors cultured 5 days in serum-free differentiation medium ± 2.5 µM inhibitors (harmine or EHT 1610) underwent flow cytometry after costaining with FITC-anti-CD41 and PI. (**A**) Mk polyploidization (PI). (**B**) Mk size (FSC). (**C**) Mk complexity/granulation (SSC). Graphs for **A-C**: mean ± SEM for 3 independent experiments. ****P* < 0.005, one way ANOVA with Tukey's post hoc test. (**D-F**) Conditionally immortalized imMKCL cells cultured 6 days in doxycycline-free differentiation medium ± 5 µM inhibitors were analyzed as in **A-C**. (**D**) Mk polyploidization (PI). (**E**) Mk size (FSC). (**F**) Mk complexity/granulation (SSC). Graphs for **D-F**: mean ± SEM for 3 independent experiments. **P* < 0.05; ****P* < 0.005; ns: not significant, one way ANOVA with Tukey's post hoc test.

Figure 3

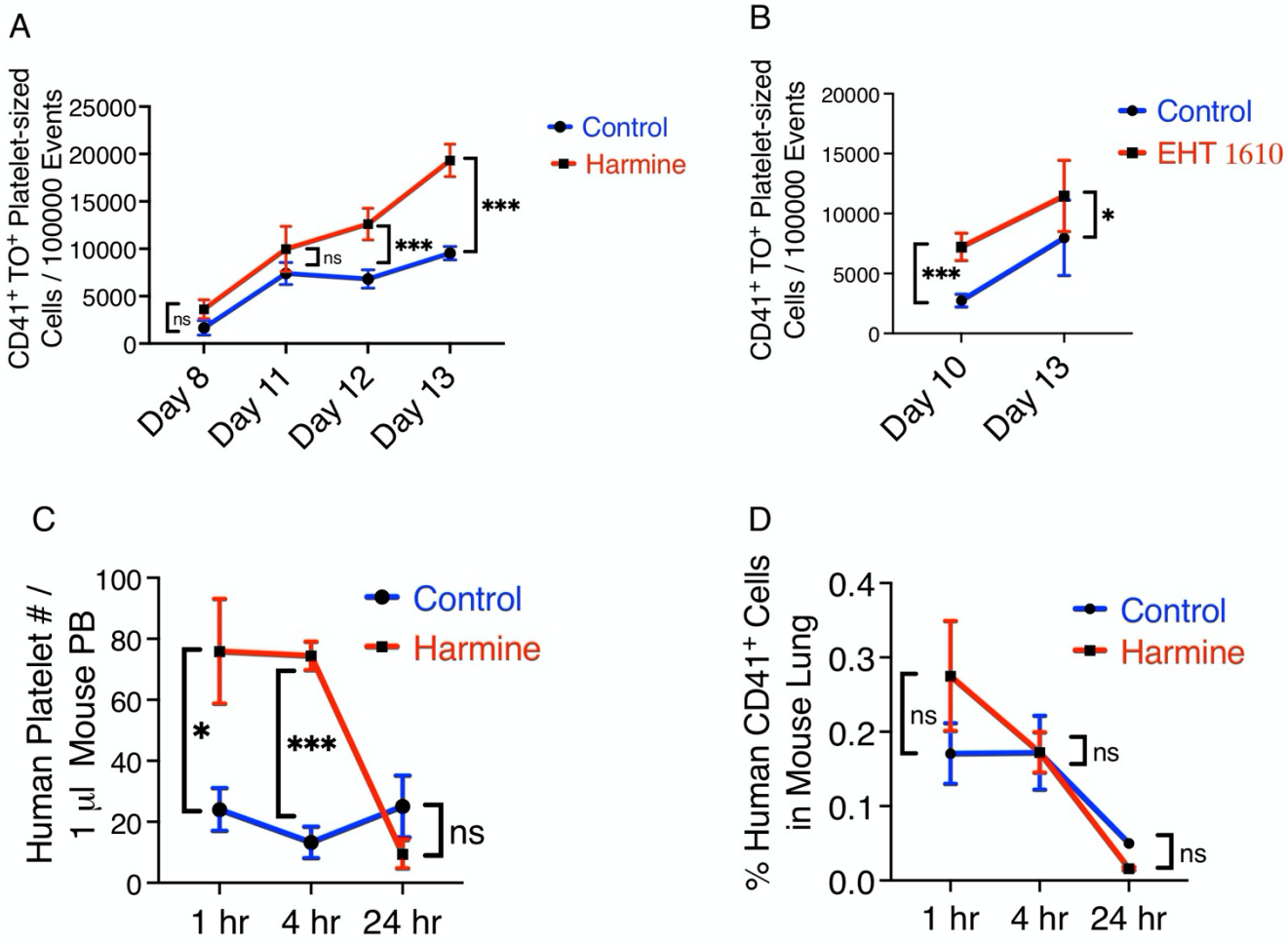

Figure 3. Enhanced platelet production by neonatal megakaryocytes (Mk) treated with Dyrk1 inhibitors. (**A-B**) *In vitro* platelet release assay. Cord blood CD34$^+$ cells were cultured up to 13 days in Mk medium ± 5 µM harmine or 2.5 µM EHT 1610. Culture supernatants underwent flow cytometry after labelling with APC-anti-CD41 and thiazole orange (TO). Gating was based on size and CD41$^+$/TO$^+$ characteristics of normal donor platelets. Graphs: mean platelet numbers ± SEM for 4 independent experiments. *P < 0.05; ***P < 0.005; ns: not significant, Student's t test. (**C**) *In vivo* platelet release. Cord blood CD34$^+$ progenitors were cultured 11 days in Mk medium ± 2.5 µM harmine. 4 x 10^6 cells were transplanted per irradiated NSG mouse. Peripheral blood samples were then evaluated for the presence of human platelets by flow cytometry with a human-specific CD41 antibody. Graph: circulating human platelet count ± SEM, n = 4–6/group. *P < 0.05; ***P < 0.005; ns: not significant, one way ANOVA with Tukey's post hoc test. (**D**) Lung entrapment of human megakaryocytes. Lung tissue was evaluated for the presence of human megakaryocytes by flow cytometry with a human-specific CD41 antibody. Graph: percent of cells expressing human CD41 ± SEM, n = 4–6/group. ns: not significant, one way ANOVA with Tukey's post hoc test.

Figure 4

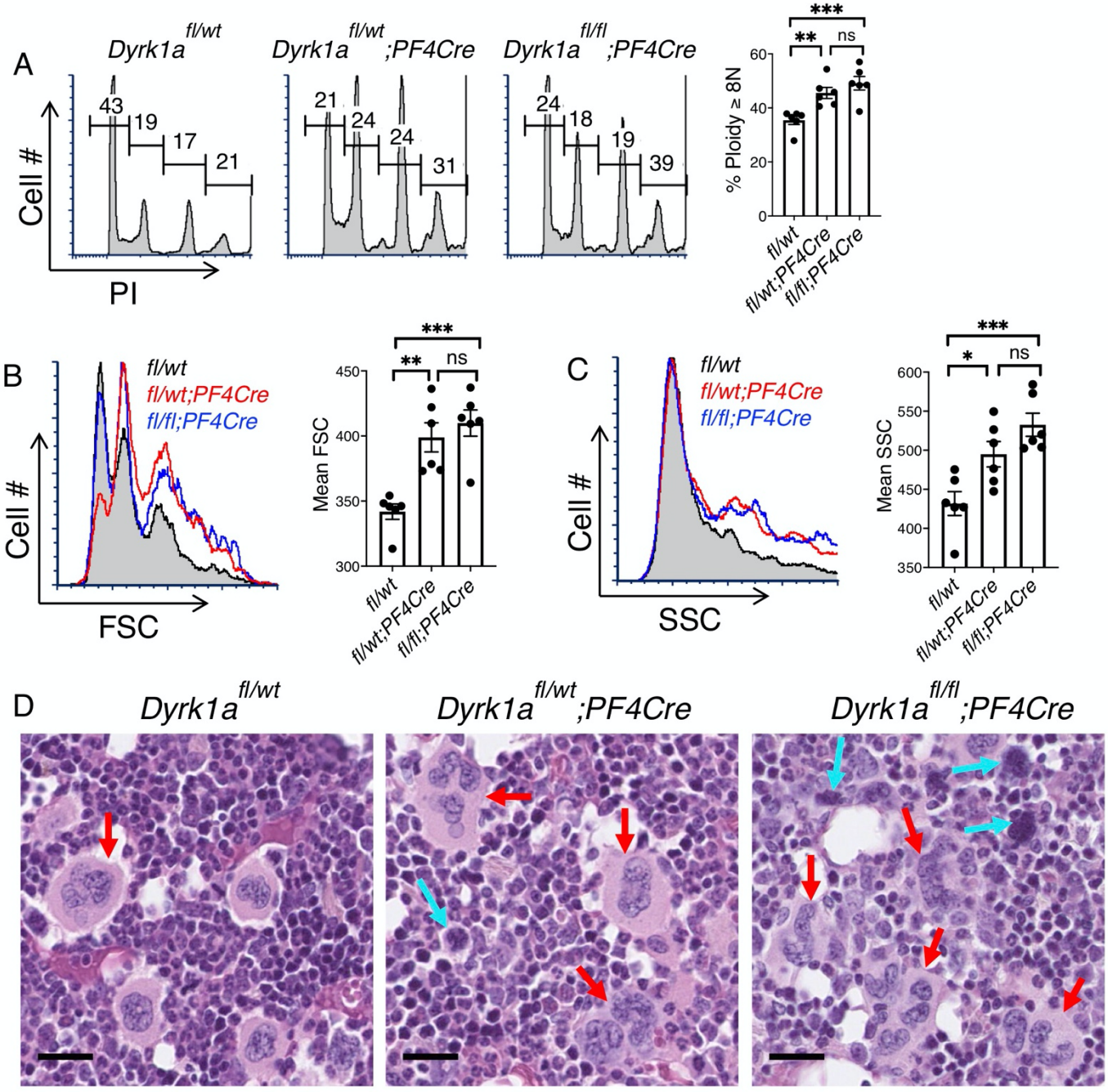

Figure 4. Implication of Dyrk1a isoform in megakaryocyte (Mk) morphogenesis. (**A-C**) Marrow samples from indicated murine strains underwent flow cytometry after costaining with FITC-anti-CD41 and PI. (**A**) Mk polyploidization (PI). (**B**) Mk size (FSC). (**C**) Mk complexity/granulation (SSC). Graphs: mean ± SEM, n = 6/group. *$P < 0.05$; **$P < 0.01$; ***$P < 0.005$; ns: not significant, one way ANOVA with Tukey's post hoc test. (**D**) Representative Mk morphology in H&E-stained marrow sections from indicated strains. Red arrows: large polyploid Mk. Blue arrows: small pyknotic Mk. Light microscopy (Hamamatsu NanoZoomer S360 scanner, original magnification x 200, scale bar 20 μm).

Figure 5

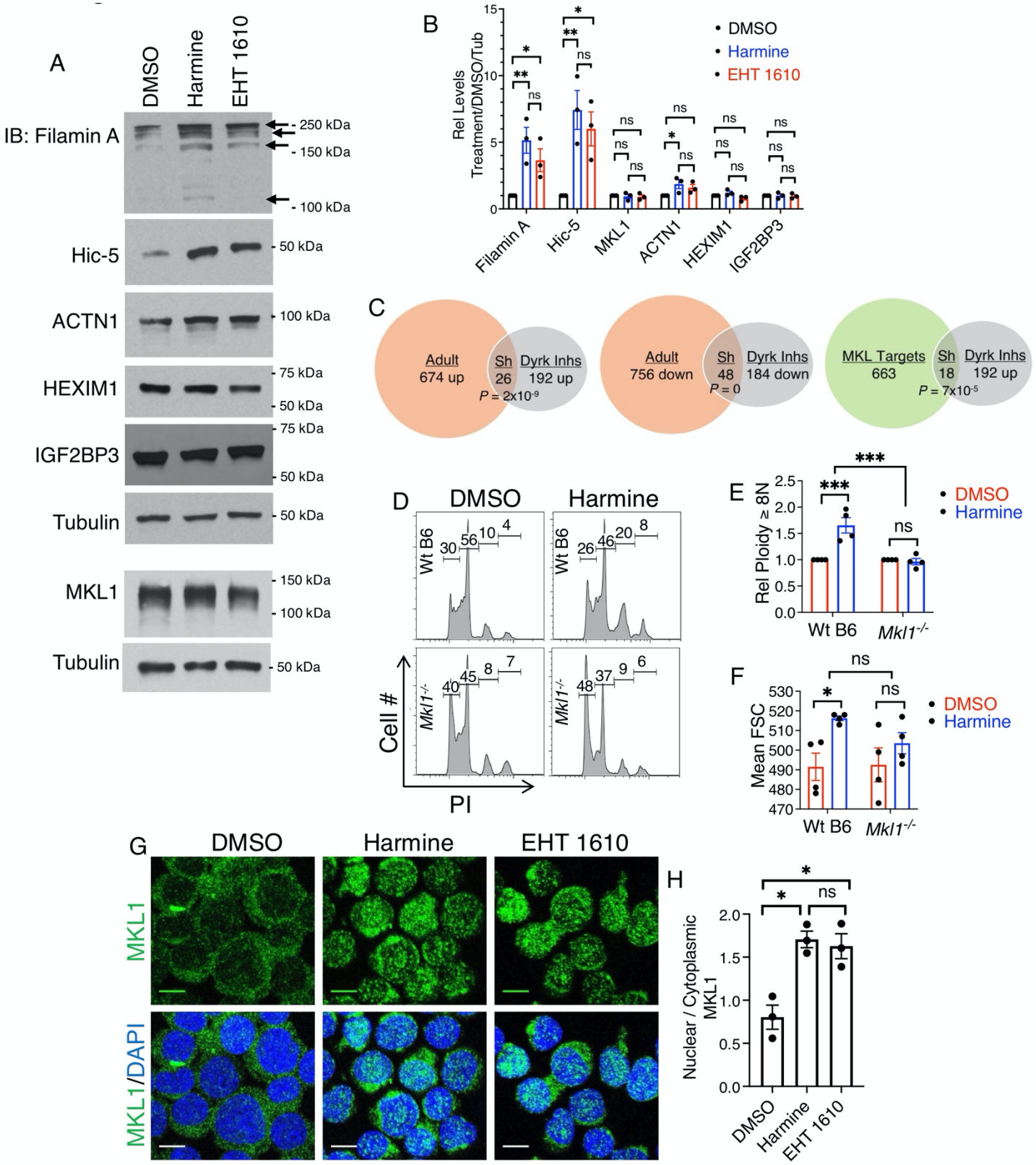
A
DMSO
Harmine
EHT 1610
IB: Filamin A
250 kDa
150 kDa
100 kDa
Hic-5
50 kDa
ACTN1
100 kDa
HEXIM1
75 kDa
50 kDa
IGF2BP3
75 kDa
50 kDa
Tubulin
50 kDa
MKL1
150 kDa
100 kDa
Tubulin
50 kDa
B
Rel Levels Treatment/DMSO/Tub
DMSO
Harmine
EHT 1610
Filamin A
Hic-5
MKL1
ACTN1
HEXIM1
IGF2BP3
C
Adult 674 up
Sh 26
Dyrk Inhs 192 up
P = 2x10-9
Adult 756 down
Sh 48
Dyrk Inhs 184 down
P = 0
MKL Targets 663
Sh 18
Dyrk Inhs 192 up
P = 7x10-5
D
DMSO
Harmine
Wt B6
Mkl1-/-
Cell #
PI
E
Rel Ploidy ≥ 8N
DMSO
Harmine
Wt B6
Mkl1-/-
F
Mean FSC
DMSO
Harmine
Wt B6
Mkl1-/-
G
DMSO
Harmine
EHT 1610
MKL1
MKL1/DAPI
H
Nuclear / Cytoplasmic MKL1
DMSO
Harmine
EHT 1610

Figure 5. MKL1 involvement in Dyrk control of megakaryocyte (Mk) morphogenesis. (**A**) Effects of Dyrk1 inhibition on targets of MKL1 and P-TEFb. Cord blood $CD34^+$ cells cultured 6 days in Mk medium ± 5 μM inhibitors underwent immunoblot (IB) of whole cell lysates. Arrows: Filamin A isoforms. (**B**) Tubulin-normalized densitometry signals from IBs as in (**A**). Graph: mean fold changes with inhibitors ± SEM for 3 independent experiments. *P < 0.05; **P < 0.01; ns: not significant, one way ANOVA with Tukey's post hoc test. (**C**) Transcriptomic effects in human megakaryocyte precursors of ontogenic stage (adult vs. neonatal) and Dyrk inhibition (neonatal ± inhibitors). $CD34^+$ cells cultured 4 days in Mk medium underwent purification of CD61+ cells followed by RNA-seq. Shown are overlapping genes (Sh) with hypergeometric P values; n = 3 independent experiments. See Supplemental Table 1 for gene lists. (**D-F**) MKL1 requirement for morphogenesis enhancement. Marrow progenitors from indicated strains cultured 3 days in murine Mk medium ± 5 μM harmine underwent flow cytometry after costaining with FITC-anti-CD41 and PI. (**D**) Mk polyploidization (PI). (**E**) Graph: relative % Mk $\geq$ 8N ± SEM, n = 4/group. ***P < 0.005; ns: not significant, 2-way ANOVA. (**F)** Mk size (FSC). Graph: mean ± SEM, n = 4/group. *P < 0.05; ns: not significant, 2-way ANOVA. (**G**) MKL1 localization. Human $CD34^+$ progenitors cultured 24 hours in Mk medium ± 5 μM inhibitors underwent immunofluorescent staining (IF) and confocal microscopy (Zeiss LSM700, original magnification x 630, scale bar 10 μm). (**H**) Graph: mean ratio nuclear/cytoplasmic MKL1 signal ± SEM for 3 independent experiments. *P < 0.05; ns: not significant, one way ANOVA with Tukey's post hoc test.

Figure 6

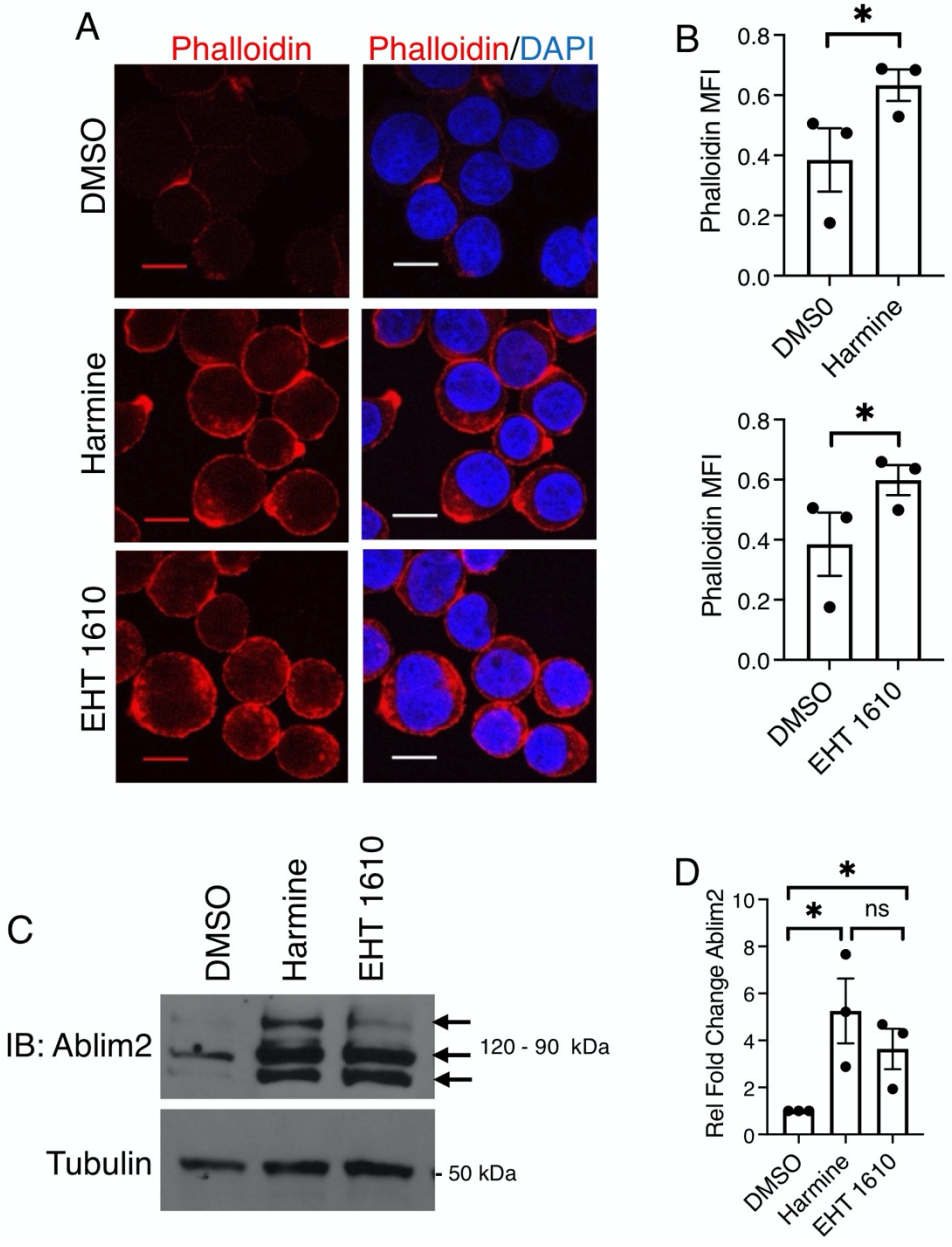

Figure 6. Changes in actin cytoskeleton and actin-associated factors in association with Dyrk1 inhibition. (**A**) Induction of filamentous actin (F-actin). Human CD34$^+$ progenitors cultured 24 hours in megakaryocyte medium ± 5 μM inhibitors underwent staining with indicated fluorescent dyes followed by confocal microscopy (Zeiss LSM700, original magnification x 630, scale bar 10 μm). (**B**) Graphs: mean fluorescent intensity (MFI) of Phalloidin-Alexa-594 signals ± SEM for 3 independent experiments as in (**A**). *P < 0.05, Student's t test. (**C**) Induction of Ablim2. Progenitors cultured 5 days as in (**A**) underwent IB of whole cell lysates. Arrows: Ablim2 isoforms. (**D**) Tubulin-normalized densitometry signals from IBs as in (**C**). Graph: mean fold changes with inhibitors ± SEM for 3 independent experiments. *P < 0.05; ns: not significant, one way ANOVA with Tukey's post hoc test.

Figure 7

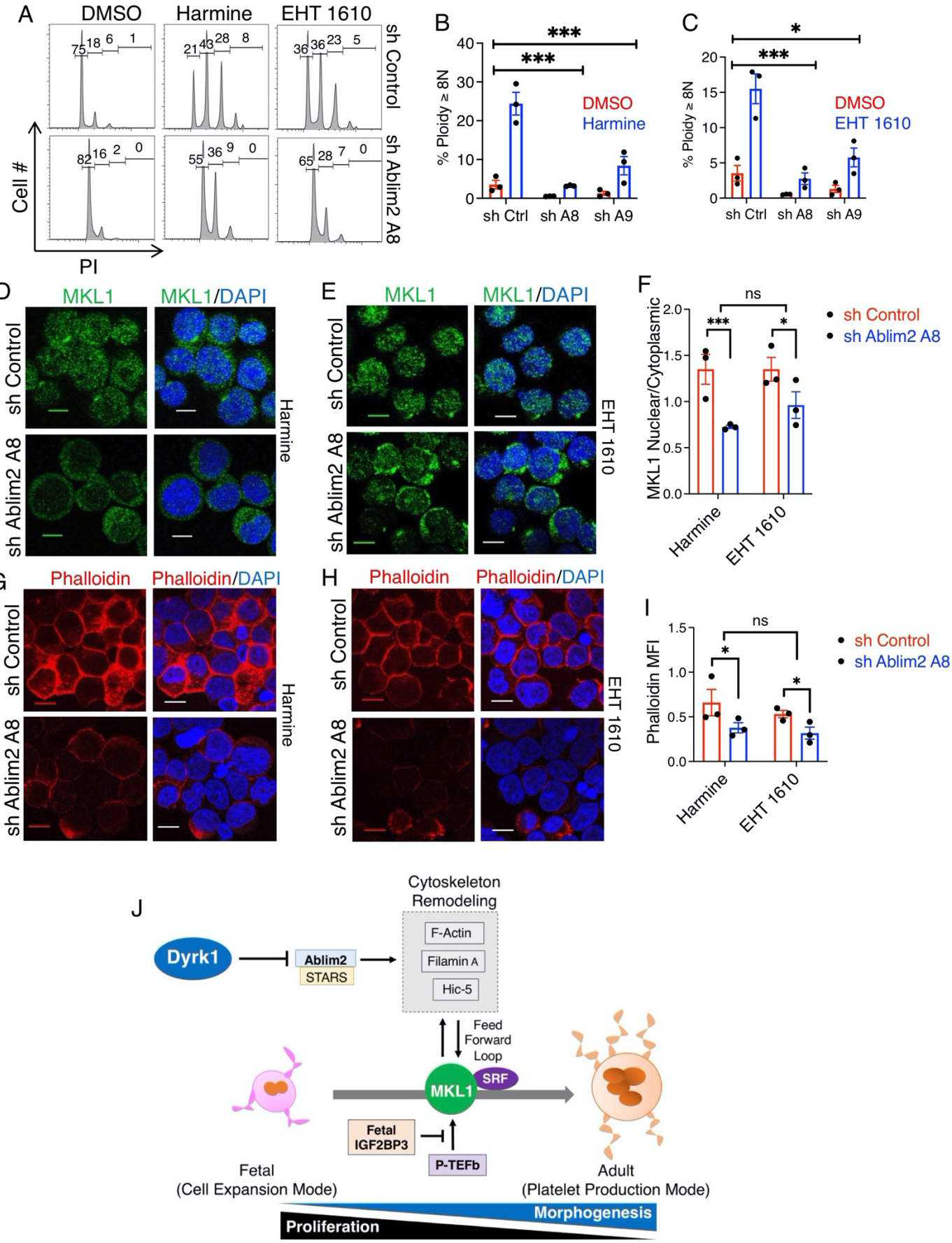
A
DMSO
Harmine
EHT 1610
sh Control
sh Ablim2 A8
Cell #
PI
B
% Ploidy ≥ 8N
DMSO
Harmine
sh Ctrl
sh A8
sh A9
C
% Ploidy ≥ 8N
DMSO
EHT 1610
sh Ctrl
sh A8
sh A9
D
MKL1
MKL1/DAPI
sh Control
sh Ablim2 A8
Harmine
E
MKL1
MKL1/DAPI
sh Control
sh Ablim2 A8
EHT 1610
F
MKL1 Nuclear/Cytoplasmic
ns
sh Control
sh Ablim2 A8
Harmine
EHT 1610
G
Phalloidin
Phalloidin/DAPI
sh Control
sh Ablim2 A8
Harmine
H
Phalloidin
Phalloidin/DAPI
sh Control
sh Ablim2 A8
EHT 1610
I
Phalloidin MFI
ns
sh Control
sh Ablim2 A8
Harmine
EHT 1610
J
Cytoskeleton Remodeling
F-Actin
Filamin A
Hic-5
Dyrk1
Ablim2
STARS
Feed Forward Loop
MKL1
SRF
Fetal IGF2BP3
P-TEFb
Fetal
(Cell Expansion Mode)
Adult
(Platelet Production Mode)
Morphogenesis
Proliferation

Figure 7. Ablim2 is a critical upstream element in megakaryocyte (Mk) morphogenesis signaling. (**A**) Impact of Ablim2 deficiency on polyploidization response. Neonatal $CD34^+$ cells transduced with control or *ABLIM2* targeting lentiviral shRNA constructs were cultured 5 days in Mk medium ± 5 μM inhibitors followed by flow cytometry as in Fig. 1A. (**B-C**) Graphs: mean % Mk $\geq$ 8N ± SEM for 3 independent experiments. *$P < 0.05$; ***$P < 0.005$, 2-way ANOVA comparing fold induction. (**D-F**) MKL1 localization. Cells transduced as in (**A**) underwent 24 hours in Mk medium ± 5 μM inhibitors followed by IF staining and confocal microscopy (Zeiss LSM700, original magnification x 630, scale bar 10 μm). (**F**) Graph: mean ratio nuclear/cytoplasmic MKL1 signal ± SEM for 3 independent experiments. *$P < 0.05$; ***$P < 0.005$; ns: not significant, 2-way ANOVA comparing fold change. (**G-I**) Induction of F-Actin. Cells as in (**D**) underwent staining with fluorescent dyes and confocal microscopy (Zeiss LSM700, original magnification x 630, scale bar 10 μm). (**I**) Graph: MFI of Phalloidin-Alexa-594 signal ± SEM for 3 independent experiments. *$P < 0.05$; ns: not significant, 2-way ANOVA comparing fold change. (**J**) Diagram of pathways influencing MKL1 in its programming of the fetal-adult megakaryocyte transition. P-TEFb (positive transcription elongation factor) signaling determines levels, and actin cytoskeleton determines function. Diagram shows the influence exerted on MKL1/SRF by Dyrk1 destabilization of the F-actin-binding factors Ablim2/STARS.

Table 1. Enrichment categories (Gene Ontology Cellular Components): genes upregulated both with Dyrk inhbitors and in adult versus neonatal megakaryocytes. Top 10 of 61 entries.

Index	Name	P-value	Adjusted P-value	Odds Ratio	Combined score
1	Contractile actin filament bundle (GO:0097517)	0.001230	0.02500	43.72	292.97
2	Stress fiber (GO:0001725)	0.001230	0.02500	43.72	292.97
3	Specific granule (GO:0042581)	0.001141	0.02500	16.46	111.55
4	Actomyosin (GO:0042641)	0.001767	0.02694	36.10	228.83
5	Zonula adherens (GO:0005915)	0.007776	0.05993	159.75	775.88
6	Specific granule membrane (GO:0035579)	0.006198	0.05993	18.62	94.65
7	Nuclear speck (GO:0016607)	0.006485	0.05993	8.76	44.14
8	Nuclear body (GO:0016604)	0.007859	0.05993	5.73	27.78
9	Myosin filament (GO:0032982)	0.01164	0.07101	99.83	444.56
10	Focal adhesion (GO:0005925)	0.01073	0.07101	7.25	32.87